THE JOURNAL OF PHYSICAL CHEMISTRY B

ARTICLE

pubs.acs.org/JPCB

Bimolecular Electron Transfer in Ionic Liquids: Are Reaction Rates Anomalously High?

Min Liang,[†] Anne Kaintz,[†] Gary A. Baker,[‡] and Mark Maroncelli*[,†]

[†]Department of Chemistry, The Pennsylvania State University, University Park, Pennsylvania 16802, United States

[‡]Department of Chemistry, The University of Missouri—Columbia, Columbia, Missouri 65211, United States

Supporting Information

ABSTRACT: Steady-state and picosecond time-resolved emission spectroscopy are used to monitor the bimolecular electron transfer reaction between the electron acceptor 9,10-dicyanoanthracene in its S_1 state and the donor *N*,*N*-dimethylaniline in a variety of ionic liquids and several conventional solvents. Detailed study of this quenching reaction was undertaken in order to better understand why rates reported for similar diffusion-limited reactions in ionic liquids sometimes appear much higher than expected given the viscous nature of these liquids. Consistent with previous studies, Stern−Volmer analyses of steady-state and lifetime data provide effective quenching rate constants k_q, which are often 10−100-fold larger than simple predictions for diffusion-limited rate constants k_D in ionic liquids. Similar departures from k_D are also observed in conventional organic solvents having comparably high viscosities, indicating that this behavior is not unique to ionic liquids. A more complete analysis of the quenching data using a model combining approximate solution of the spherically symmetric diffusion equation with a Marcus-type description of electron transfer reveals the reasons for frequent observation of $k_q \gg k_D$. The primary cause is that the high viscosities typical of ionic liquids emphasize the transient component of diffusion-limited reactions, which renders the interpretation of rate constants derived from Stern−Volmer analyses ambiguous. Using a more appropriate description of the quenching process enables satisfactory fits of data in both ionic liquid and conventional solvents using a single set of physically reasonable electron transfer parameters. Doing so requires diffusion coefficients in ionic liquids to exceed hydrodynamic predictions by significant factors, typically in the range of 3−10. Direct, NMR measurements of solute diffusion confirm this enhanced diffusion in ionic liquids.

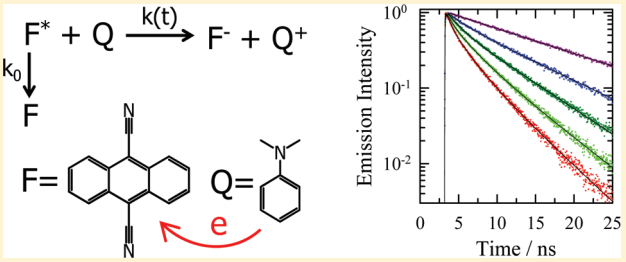

1. INTRODUCTION

Among the myriad uses for which ionic liquids are currently being investigated, numerous applications fall within the area of energy generation and storage.[1] For example, the low volatility, intrinsic conductivity, and tailorability of ionic liquids afford significant advantages over conventional organic solvents in devices such as fuel cells,[2] supercapacitors,[3,4] batteries,[2,5] and dye-sensitized solar cells.[6,7] Electron transfer is a key component of many such applications, and for this reason, it is important to achieve a sound understanding of the nature of electron transfer processes in ionic liquids. In particular, it is important to learn to what extent the theoretical approaches developed for treating electron transfer in conventional solvents are also applicable to ionic liquids. Toward this end many electrochemical studies of heterogeneous electron transfer have been performed.[8,9] These studies have shown that while the mechanisms of reaction are typically the same as in high-polarity conventional solvents, the high viscosities of ionic liquids usually produce much slower rates. Some interesting attempts have been made to relate heterogeneous reaction kinetics to fundamental theories of electron transfer,[10] but the largely unknown and apparently complex structure of ionic liquid−electrode interfaces[11] renders comparison to theory difficult. In the case of homogeneous electron transfer, simulations[12−15] and recent experimental studies of photoinduced intramolecular processes[16,17] suggest that electron transfer is comparable in ionic liquids and high-polarity conventional solvents. The primary difference found in ionic liquids is a marked decrease in rates caused by the much slower and highly dispersed solvation dynamics characteristic of these solvents.[18,19]

Bimolecular electron transfer reactions, the subject of the present work, have been previously studied by several groups.[17,20−30] In a number of cases, the rates of reactions known to be diffusion limited in conventional solvents show what on first glance appear to be anomalously high rates in ionic liquids. Table 1 documents some of the results currently available. In one of the earliest studies (#8 in Table 1), McLean et al. measured the electron transfer quenching of triplet benzophenone in five ionic liquids and two conventional solvents as a function of temperature.[21] Whereas the rates observed in the solvents acetonitrile and

Received: November 12, 2011
Revised: December 18, 2011
Published: December 22, 2011

Table 1. Prior Results on Diffusion-Limited Bimolecular Electron Transfer Reactions in Ionic Liquids

#	reaction[a]	ionic liquids[b]	η (cP)[(c)]	[Q] (mol dm^{-3})[(c)]	τ_0 (ns)[(c)]	k_q/k_D[(c)]	technique[(d)]	ref
1	C15n* + DMA → C15n$^-$ + DMA$^+$	$[Im_{51}][BF_4]$	135	0.5−1.5	1−4	100−170	ps FL	30
2	C15n* + DMA → C15n$^-$ + DMA$^+$	$[Im_{21}][Tf_2N]$	31	0.05−0.25	1−3	5−8	ps FL	28
3	C15n* + DMA → C15n$^-$ + DMA$^+$	DAF	75	0.01−0.08	1−3	33−35 130−150	ps FL SS FL	27
4	BPH* + CCl_4 → BPH$^+$ + CCl_4^-	$[Im_{41}][Tf_2N]$	49	0.01−0.12	5	16	ns TA	29
5	DCA* + D → DCA$^-$ + D$^+$	$[Im_{n1}][PF_6]$ n = 4,8	350, 570	0.4−1.1	12, 13	85, 150	SS FL	26
6	Py* + DMA → Py$^-$ + DMA$^+$	4 Im ILs	34−330	0.01−0.06	300	2−4	ns FL and TA	25
7	BuPy$^\bullet$ + DQ → BuPy$^+$ + DQ$^{\bullet-}$	5 N and Pr ILs	80−700	<.004	~5 × 10^4	5−14	radiolysis	22
8	^{3}Bp* + Naph → Bp + ^{3}Naph*	5 Im ILs	50−700	<.003	>2000	3−12	ns TA	21

[a] C15n = various coumarin dyes (151, 152, ...); DMA = *N*,*N*-dimethylaniline; BPH = benzophenone ketyl radical; DCA = 9,10-dicyanoanthracene; D = various amine donors; Py = pyrene; MV = methylviologen; BuPy = *n*-butylpyridine; DQ = duraquinone; Bp = benzophenone; and Naph = naphthalene. [b] Im_{n1} designates a methylimidazolium cation with a C_nH_{2n+1} substituent. DAF = *N*,*N*-dimethylethlyammonium formate, and Im, N, and Pr, respectively, denote imidazolium, ammonium, and pyrrolidinium ionic liquids. [(c)] η denotes solvent viscosity, [Q] the quencher (abundant reactant) concentration, τ_0 the fluorophore (rare reactant) lifetime in the absence of quencher, k_q the observed bimolecular rate constant, and k_D the rate constant calculated from $k_D = 8k_BT/3\eta$. [(d)] FL = fluorescence; SS = steady state; and TA = transient absorption

toluene were close to expectations for a diffusion-limited process, $k_D = 8k_BT/3\eta$ (where k_B is Boltzmann's constant, T the temperature, and η the solution viscosity) McLean et al. noted that the rates in ionic liquids were up to an order of magnitude larger. Similar observations were made in another early study by Skrzypczak and Neta[22] (#7 in Table 1) who measured rates of electron transfer between the butylpyridinyl radical and duraquinone to be 5−14 times larger than expected based on viscosity-scaling rates observed in conventional solvents. Skrzypczak and Neta proposed that these high rates were the result of reactants diffusing more rapidly than would be expected based on the high bulk viscosities of ionic liquids. But enhanced diffusion alone is unlikely to account for some of the very high values of k_q/k_D shown in Table 1. For example, using a Stern−Volmer analysis of steady-state fluorescence data on the electron transfer quenching of S_1 9,10-dicyanoanthracene by amine donors, Viera and Falvey reported values of $k_q/k_D > 50$ in two high-viscosity ionic liquids.[26] Similarly high values were reported in independent studies of the fluorescence quenching of excited coumarin dyes by the groups of Sarkar (#3 in Table 1) and Bhattacharyya (#1). There are also several cases (#2 and #6) in which neutral solutes show only modest rate enhancements compared to expectations. In addition, in one study (#3 in Table 1), Stern−Volmer analysis of steady-state and time-resolved fluorescence data produced very different bimolecular rate constants. To date, no explanation for these varied results has been offered, and it is far from clear what it is about the ionic liquid environment that sometimes produces unexpectedly high bimolecular electron transfer rates.

In the present study, we take a closer look at these issues and attempt to explain some of the apparently anomalous behavior observed. We report steady-state and time-resolved fluorescence measurements of the electron transfer quenching of excited-state 9,10-dicyanonanthracene (DCA) by *N*,*N*-dimethylaniline (DMA) in ionic liquids and conventional solvents. The DCA + DMA system was chosen in part because of the extreme values of (k_q/k_D) reported by Viera and Falvey[26] for strong electron donors like DMA. The long lifetime (~13 ns) of DCA and the fact that this solute shows only a very small dynamic Stokes shift also prove useful in the present work. The sort of data we collect in ionic liquids is qualitatively similar to what has been reported in previous studies. One distinction from prior work is that, in addition to measuring the reaction in low viscosity conventional solvents, we also made measurements in mixtures of ethylene glycol + glycerol, which have viscosities and polarities comparable to those of ionic liquids. These mixture data show that the anomalies reported in ionic liquids are due in large part to their high viscosities rather than being a special aspect of electron transfer in ionic media. We also for the first time measure diffusion rates of one of the species involved in the reaction (DMA) using NMR techniques. These measurements and more extensive work on other solutes[31] show that diffusion of neutral solutes of moderate size in ionic liquids is typically faster than hydrodynamic predictions but usually only by factors of 3−5. Thus, enhanced diffusion rates do account for some of the departure of k_q from k_D, but other factors are equally important.

The main way in which the present work differs from previous ionic liquid studies is that we attempt a much more detailed analysis of the bimolecular electron transfer reaction. Instead of simply applying Stern−Volmer analyses[32] to determine quenching rate constants for comparison to the diffusion limit k_D, we fit time-resolved emission decays to a complete model which couples a classical Marcus description of the distance-dependent electron transfer process[33] to a Smoluchoski-type spherical diffusion + reaction equation[34,35] to model the overall population kinetics. This sort of modeling has been applied previously by the groups of Tachiya,[36−39] Fayer,[40−42] and most recently Grampp[43−45] to understand bimolecular electron transfer in conventional solvents. Rather than solving the reaction-diffusion equations numerically as done by these other groups, we employ the convenient analytical approximations derived recently by Dudko and Szabo.[46] To our knowledge, this is the first time that their method has been employed to model experimental data. We find that it is possible to satisfactorily model all of the experimental quenching data collected in high polarity conventional solvents and ionic liquids using a single set of physically sensible parameters. This modeling makes it clear that theories developed to treat electron transfer and diffusion-limited reaction in conventional solvents apply equally well in ionic liquids. Once the much higher viscosities and the poorer approximation provided by hydrodynamic predictions for diffusion are accounted for, the rates of bimolecular electron transfer reactions in ionic liquids no longer appear anomalous.

2. EXPERIMENTAL METHODS

9,10-Dicyanoanthracene (DCA) was obtained from TCI-America (97%) and was recrystallized from a mixture of pyridine + acetonitrile

prior to use. *N*,*N*-Dimethylaniline (DMA; 99.5+%), cyclohexane and acetonitrile (HPLC grade), ethylene glycol (99.8%), and glycerol (99.5%) were obtained from Sigma-Aldrich and were used as received. The series of *N*-alkyl-*N*-methylpyrrolidinium bis(trifluoromethylsulfonyl)imides, $[Pr_{n1}][Tf_2N]$ with $n = 3, 4, 6, 8$, and 10, were prepared as described in ref 47. Propyltrimethylammonium bis(trifluoromethylsulfonyl)imide, $[N_{3111}][T_2fN]$, obtained from Kanto Chemical, and 1-butyl-3-methylimidazolium hexafluorophosphate $[Im_{41}][PF_6]$ from Iolitec (99%) were used as received except for drying. Decyltrimethylammonium bis(perfluoroethanesulfonyl)imide, $[N_{10,111}][Beti]$, was obtained by metathesis of the bromide salt (TCI America 99+%) and [Li][Beti] (3 M Corporation) following established procedures.[48] ^{1}H NMR (400 MHz, $CDCl_3$, δ_H/ppm relative to solvent residual peak): 3.26 (t, 2H), 3.12 (s, 9H), 1.72 (m (broad), 2H), 1.34 (s (br), 4H), 1.26 (s (br), 10H), 0.88 (t, 3H). Finally, trihexyltetradecylphosphonium bis(trifluoromethylsulfonyl)imide ($[P_{14,666}][Tf_2N]$) was prepared as described in ref 16. All of the ionic liquids were dried under vacuum at 45 °C overnight prior to measurement. The water contents were measured using a Mettler-Toledo DL39 Karl Fischer coulometer and were below 100 ppm by weight. Mixtures of ethylene glycol + glycerol were made by weight and had water contents of <250 ppm.

Samples for optical spectroscopy were prepared in a nitrogen-purged glovebox using a stock solution of the fluorophore DCA in cyclohexane. The cyclohexane was removed by evacuation prior to solvent addition. The optical densities of these samples were maintained near 0.1 in 1 cm quartz cuvettes. Aliquots of the quencher DMA were added directly to the cuvette samples using a micropipet. Estimated uncertainties in the DMA concentration are between 16−6% over the range 0.05−0.3 M. All optical measurements were maintained at constant temperature, usually 298 K ± 0.1 K.

Steady-state absorption spectra were measured using a Hitachi U-3000 UV/vis spectrometer at 1 nm resolution and steady-state fluorescence spectra recorded with a SPEX Fluorolog 212 spectrometer (2 nm). Emission spectra were corrected for detector sensitivity using a method based on a series of dye standards.[49] Time-resolved fluorescence data were recorded using a home-built time-correlated single photon counting (TCSPC) setup.[50] The excitation source (420 nm) was the doubled output of a cavity-dumped Ti:sapphire laser (Coherent Mira 900F + APE PulseSwitch) operating at a repetition rate of 3 MHz. Fluorescence was collected at magic angle with respect to the excitation polarization through a monochromator (ISA H10) with an emission bandpass of 4 nm. The instrumental response of this setup was 25−30 ps (fwhm) as judged by the signal from a scattering solution. Fluorescence decays having greater than 5000 peak counts were collected over time windows of between 8 and 45 ns in 4096 channels depending on sample lifetime. Decays were fit to multiexponential functions using a convolute-and-compare algorithm. Three decays were typically measured for each sample and an averaged multiexponential description used for analysis as described later.

The viscosities of the ionic liquid solutions and ethylene glycol + glycerol mixtures were measured with a Brookfield Model HBDV-III+CP cone/plate viscometer calibrated using the NIST-certified viscosity standards N75 and N100 (Cannon Instruments). In most cases, viscosities were measured from 5 to 65 °C with an increment of 5 °C and fit to the Vogel−Fulcher−Tammann equation. A summary of these viscosity data is provided in the Supporting Information.

Diffusion coefficients of DMA were determined from ^{1}H data measured on Bruker DRX-400 and AV-III-850 spectrometers using the longitudinal eddy current delay stimulated echo pulse sequence with bipolar gradient pulses.[51] In the case of the $[Pr_{n1}][Tf_2N]$ series of ionic liquids, diffusion measurements were made on DMA solutions at a series of concentrations between 0 and 0.3 M and diffusion coefficients extrapolated to infinite dilution. In this manner, it was found that diffusion coefficients measured with 50 mM DMA are within uncertainties (±5%) of the limiting values. Diffusion coefficients of DMA in other solvents were therefore determined only at 50 mM concentrations. Representative data are provided in the Supporting Information.

Scheme 1

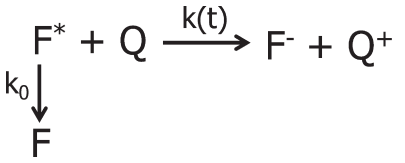

3. MODELING THE TIME-DEPENDENT QUENCHING PROCESS

3.1. Formalism. We assume quenching to be the result of irreversible electron transfer between an excited fluorophore F^* (DCA* here, an electron acceptor) and a quencher Q (DMA, the donor) as depicted in Scheme 1. Measured fluorescence decays $I(t)$ are related to the time-dependent reaction rate coefficient $k(t)$[52] via

$$\frac{I(t)}{I(0)} = \frac{[F^*(t)]}{[F^*(0)]} = \exp\{-k_0 t - [Q]\int_0^t k(t')\mathrm{d}t'\} \quad (1)$$

where $[Q]$ indicates the concentration of quencher, and k_0 is the fluorescence decay rate constant in the absence of Q. $k(t)$ is determined from the spherically symmetric reaction−diffusion equation for the F^*−Q pair distribution $p(r,t)$[34,35,43]

$$\frac{\partial p(r,t)}{\partial t} = \left\{D\frac{1}{r^2}\frac{\partial}{\partial r}r^2 \exp[-\beta w(r)]\frac{\partial}{\partial r}\exp[+\beta w(r)] - \kappa(r)\right\}p(r,t) \quad (2)$$

where D is the relative diffusion coefficient of F and Q, assumed to be given by the sum of their individual diffusion coefficients, $w(r)$ is the potential of mean force between F and Q, $\beta = (k_B T)^{-1}$, where $\kappa(r)$ is the function that describes how the reaction rate varies with the F^*−Q separation r. (We do not distinguish between F and F^* with regard to interaction potentials or diffusion.) Finally, $p(r,t)$ and $k(t)$ are related by

$$k(t) = 4\pi\int_0^\infty r^2 p(r,t)\kappa(r)\mathrm{d}r \quad (3)$$

Exact solution of eq 2 for $k(t)$ is only possible in a few simple cases,[53] which do not include $\kappa(r)$ models appropriate for electron transfer quenching.

Before discussing solution of eq 2, we digress briefly to discuss one simplified model which does afford analytic results important for later discussion. In the absence of significant $F-Q$ interactions and for $\kappa(r)$ such that reaction occurs instantaneously at some contact distance σ but not elsewhere, solution of eq 2 provides the prediction first obtained by Smoluchowski[54]

$$k(t) = k_D\left\{1 + \sqrt{\frac{\sigma^2}{\pi Dt}}\right\} \tag{4}$$

which integrates to

$$\frac{I(t)}{I(0)} = \exp\{-k_0 t - [Q](k_D t + 8\sigma^2\sqrt{\pi Dt})\} \tag{5}$$

with $k_D = 4\pi\sigma D$. If one can ignore the $\sqrt{t}$ or transient term in eq 4, single exponential emission decays are predicted, and Stern−Volmer type of analyses[32] of either steady-state emission intensities or emission lifetimes as functions of quencher concentration yield a bimolecular rate constant equal to k_D. In conventional liquids, the value of k_D can be evaluated with moderate accuracy using the Stokes−Einstein prediction for diffusion coefficients, $D = k_B T/6\pi\eta R$, where η is the solvent viscosity and R the radius of the diffusing molecule. Denoting the radii of F and Q by R_F and R_Q and assuming $\sigma = R_F + R_Q$, one obtains what we will hereafter refer to as the simple Smoluchowski prediction for the diffusion-limited rate constant[55,56]

$$k_D = \frac{8k_B T}{3\eta}\left(\frac{(R_F + R_Q)^2}{4R_F R_Q}\right) \tag{6}$$

For comparably sized F and Q molecules, the term in parentheses in eq 6 is close to unity, and one has the remarkably simple prediction $k_D = 8k_B T/3\eta$ used in Table 1.

Returning now to the more general case, to solve eq 2 for $k(t)$, we rely on the approximate solution proposed by Dudko and Szabo.[46,57] These authors showed that $k(t)$ can be approximately expressed

$$k(t) = k(\infty)[1 + \alpha_1 e^{\gamma_1^2 t}\,\mathrm{erfc}(\sqrt{\gamma_1^2 t}) + \alpha_2 e^{\gamma_2^2 t}\,\mathrm{erfc}(\sqrt{\gamma_2^2 t})] \tag{7}$$

where the long-time limiting rate constant

$$k^{-1}(\infty) = \langle\kappa\rangle^{-1} + k_{DC}^{-1}(\infty) \tag{8}$$

is a composite of the reaction-limited rate constant $\langle\kappa\rangle$, given by

$$\langle\kappa^n\rangle = \int_0^\infty 4\pi r^2\, e^{-\beta w(r)}\,\kappa^n(r)\mathrm{d}r \tag{9}$$

with $n = 1$, and the long-time diffusion-controlled (DC) rate constant

$$k_{DC}(\infty) = \frac{\frac{D}{4\pi}\langle\kappa\rangle^2}{\int_0^\infty \frac{e^{+\beta w(r)}}{r^2}\left(\int_0^r x^2\kappa(x)\, e^{-\beta w(x)}\,\mathrm{d}x\right)^2\mathrm{d}r} \tag{10}$$

The time-dependent portion of $k(t)$ is written in terms of the parameters[57]

$$\gamma_{1,2} = (\mu \mp \lambda)\frac{\langle\kappa^2\rangle}{\langle\kappa\rangle^2} \quad \text{and} \quad \alpha_{1,2} = \frac{\langle\kappa\rangle}{2k_{DC}(\infty)}\left(1 \pm \frac{\mu}{\lambda}\right) \tag{11}$$

where

$$\mu = \frac{k_{DC}^2(\infty)}{8\pi D^{3/2}} \quad \text{and} \quad \lambda^2 = \mu^2 - [\langle\kappa\rangle + k_{DC}(\infty)]\frac{\langle\kappa\rangle^2}{\langle\kappa^2\rangle} \tag{12}$$

Dudko and Szabo tested these expressions against numerical solutions of eq 2.[53] In the case of contact reactions (reaction only at $r = \sigma$ as described above), they found this approximation to be within a few percent of numerical solutions of eq 2 for a wide range of system parameters. In cases in which reaction occurs over a substantial range of distances, they found more modest accuracies in the range 10−15%. Given that the distance dependence of electron transfer can only be treated semiquantitatively, we view this level of accuracy appropriate to our purposes.

The distance dependence of the quenching reaction is assumed to be described by the semiclassical form of the Marcus expression for nonadiabatic electron transfer[58,59,33]

$$\kappa = \frac{V_{el}^2}{h}\left(\frac{1}{4\pi\lambda k_B T}\right)^{1/2}\exp\left\{-\frac{(\Delta G + \lambda)^2}{4\lambda k_B T}\right\} \tag{13}$$

where V_{el} is the electronic coupling, λ the reorganization energy, and ΔG the driving force for reaction. All three of these quantities depend upon the separation between F^*-Q, and we represent these dependences as follows. The electronic coupling is assumed to decrease exponentially with distance as

$$V_{el}^2(r) = V_0^2\exp\{-\beta_{el}(r - r_0)\} \tag{14}$$

where $r_0 = R_F + R_Q$ and β_{el} the decay constant. The reorganization energy consists of an intramolecular contribution and a solvent contribution $\lambda(r) = \lambda_{intra} + \lambda_{solv}(r)$. For the solvent contribution, we use the 2-sphere dielectric continuum expression of Marcus[60,61]

$$\lambda_{sol}(r) = \frac{e^2}{(4\pi\varepsilon_0)}\left\{\frac{1}{2R_F} + \frac{1}{2R_Q} - \frac{1}{r}\right\}\left\{\frac{1}{n^2} - \frac{1}{\varepsilon_r}\right\} \tag{15}$$

where ε_0 is the permittivity of free space, n the refractive index, and ε_r the relative permittivity of the solvent. For the distance dependence of the driving force, we adopt the Rehm−Weller expression[62]

$$\Delta G(r) = \Delta G_0 - \frac{e^2}{(4\pi\varepsilon_0)\varepsilon_r}\frac{1}{r} \tag{16}$$

where ΔG_0 is the free energy of reaction.

3.2. Specification of Model Parameters. Application of the model just described requires specification of a number of parameters characterizing the reactants, the electron transfer process, and the solvent. For convenience, these parameters are summarized in Table 2. Choice of values for these parameters is discussed below.

dx.doi.org/10.1021/jp210892c |J. Phys. Chem. B 2012, 116, 1370–1384

Table 2. Summary of Model Parameters Used in Fitting Quenching Data

parameter	value	use in fits
R_F: fluorophore radius	3.66 Å	fixed
R_Q: quencher radius	3.12 Å	fixed
λ_{intra}: intramolecular reorganization energy	0.4 eV	fixed
V_0: electronic coupling at $r = R_F + R_Q$	100 cm^{-1}	initially varied
β_{el}: coupling length scale parameter	1.5 $Å^{-1}$	fixed
ε_r: relative permittivity	39 (or 2.0)[a]	fixed
n: refractive index	1.42	fixed
ΔG_0: free energy change	−1.2 (or +0.8)[a] eV	varied
τ_0: unquenched lifetime	10−14 ns	fixed at [Q] = 0 value
σ_{FQ}: size parameter of $w(r)$	$R_F + R_Q$	fixed
ε_{FQ}: energy parameter of $w(r)$	∼2.5 kJ/mol	varied
R_h: effective hydrodynamic radius	∼1.7 Å	varied

[a] Values in parentheses are used only in the case of the cyclohexane solvent.

The fluorophore and quencher radii R_F and R_Q were determined assuming spherical shapes and the van der Waals volumes[63] of DCA and DMA. The intramolecular reorganization energy was set at $\lambda_{intra} = 0.4$ eV based upon values obtained from gas-phase calculations of isolated DCA and DMA at the B3LYP/6-31G(d) and MP2/6-31G(d,p) levels.[64] The value of V_0, the electronic coupling at the contact distance $R_F + R_Q$, is a poorly defined quantity because this coupling is strongly dependent upon the relative orientations of the F^*-Q pair in addition to the their separation.[65−67] Computational studies[65−67] and analyses of experimental data on similar systems[36,43,44] suggest V_0 to be on the order of 100 cm^{-1} (12 meV). We examined the effect that varying this parameter had on fits to the observed quenching kinetics and ultimately fixed the value at 100 cm^{-1}. Experimental and computational work suggests that the decay constant β_{el} should lie within the range $1.0 \le \beta_{el} \le 2.0$ $Å^{-1}$ for most solvents.[68−70,65] We adopted a fixed value of $\beta_{el} = 1.5$ $Å^{-1}$ for all of the solvents studied here.

The reaction free energy can be estimated using the measured oxidation potential $E(Q/Q^+)$ of the donor Q and the reduction potential $E(F/F^-)$ and 0−0 transition frequency E_{00} of the acceptor F via the following relationship:[62]

$$\Delta G_0 = E(Q/Q^+) - E(F/F^-) - E_{00} \qquad (17)$$

Averages over reported literature values[71−73] are $E(F/F^-) = -0.95$ eV (vs SCE) and $E_{00} = 2.89$ eV for DCA in acetonitrile. The oxidation potential of DMA is $E(Q/Q^+) = 0.74$ eV (vs SCE),[73−76] which together provide the value $\Delta G_0 = -1.20 \pm 0.10$ eV in acetonitrile. ΔG_0 has not been measured in other solvents, but we anticipate that it will be close to −1.2 eV in all of the solvents studied here except for cyclohexane.

The solvent dependence of ΔG_0 is due to differences in the solvation energies of the separated reactants and products. It can be estimated by assuming negligible differences for the neutral species and using the Born equation for the solvation free energies of the ions

$$\Delta_{solv}G_i = -\frac{e^2}{4\pi\varepsilon_0}\left(1 - \frac{1}{\varepsilon_r}\right)\frac{1}{2R_i} \qquad (18)$$

The difference between the driving force in a solvent x compared to the reference solvent (acetonitrile) is then

$$\Delta G_0^x - \Delta G_0^{ref} = \frac{e^2}{8\pi\varepsilon_0}\left(\frac{1}{\varepsilon_r^x} - \frac{1}{\varepsilon_r^{ref}}\right)\left(\frac{1}{R_F} + \frac{1}{R_Q}\right) \qquad (19)$$

At 298 K, the relative permittivities of the conventional solvents examined here are $\varepsilon_r = 35.9$, 37.7, 42.5, and 2.02 for acetonitrile, ethylene glycol, glycerol, and cyclohexane, respectively. Equation 19 predicts negligible (0.02 eV) differences between the three polar solvents but a value of $\Delta G_0 = +0.8$ eV in cyclohexane.

The relative permittivities of only two of the ionic liquids examined here have been reported to date: $\varepsilon_r = 14.7$ and 14.0 for $[Pr_{41}][Tf_2N]$ and $[Im_{41}][PF_6]$, respectively (298 K).[77] The values of most of the other ionic liquids are expected to be similar to these values and to fall within the range $10 \le \varepsilon_r \le 15$. Use of such values in eq 19 would predict ΔG_0 to be 0.2−0.3 eV less negative in ionic liquids compared to acetonitrile, but it is not appropriate to use these permittivities in eq 19 or in eqs 15 and 16 to estimate solvation energies.[78] A variety of experiments[79−82] and simulations[13,12,83] have shown that electrostatic solvation energies in ionic liquids are typically close to those in high-polarity conventional solvents like acetonitrile. (Rather than $\varepsilon_r \approx 14$, $\varepsilon_r = \infty$ is more appropriate for these conducting solvents.[84]) In addition, Castner and co-workers[85,86] have used cyclic voltammetry to measure ΔG_0 for reactions between DCA and two variants of DMA in acetonitrile and the ionic liquid $[Pr_{41}][Tf_2N]$. They find nearly identical values, $-1.2 \le G_0 \le -1.1$ eV, which are within uncertainties of our estimates for the DCA + DMA reaction in acetonitrile. For these reasons, we expect ΔG_0 to be close to −1.2 eV in all of the ionic liquid solvents as well as the conventional polar solvents examined here. We therefore use $\Delta G_0 = -1.2$ eV as a starting point for all solvents except cyclohexane, for which we adopt the value $\Delta G_0 = +0.8$ eV.

For determining distance-dependent reorganization energies (eq 15) and driving forces (eq 16), the same problem arises with respect to use of measured values of ε_r for ionic liquids. For calculating $\lambda_{solv}(r)$ and $\Delta G(r)$, we assume that these quantities are nearly the same in all of the high-polarity solvents studied, and for simplicity, we represent these quantities using an average set of dielectric parameters $\varepsilon_r = 39$ and $n = 1.42$ for all solvents except for cyclohexane ($\varepsilon_r = 2.02$). We recognize the fact that λ_{solv} and ΔG are not likely to be strictly constant in the dipolar and ionic liquids studied here. On the basis of the measurements of the solvation energies associated with the S_0-S_1 transition of coumarin 153,[82] we expect that solvation free energies will vary by 5−10% and reorganization energies by ∼20% across this collection of solvents. In the absence of a more accurate way to assign these quantities, we use eqs 15 and 16 with fixed values of ε_r and n to provide reasonable first approximations and then allow for some variation of ΔG_0 if needed.

The potential of mean force, $w(r)$ in eq 2, is related to the radial distribution function $g_{FQ}(r) = \exp\{-w(r)/k_BT\}$ that describes the nonuniform distribution of F and Q molecules prior to initiation of the reaction. In the case of spherical solutes and solvents, radial distribution functions exhibit a characteristic peak in relative probability near to the contact distance, followed by a tail, which oscillates periodically about unity. For polyatomic solvents and solutes of arbitrary shape, radial distribution functions based on center-of-mass distances are much less coherently structured.[83,87] A broadened first peak in $g_{FQ}(r)$ is still found near

some average contact distance, but the oscillations at larger separations tend to be averaged out by the many relative orientations of F and Q molecules. We represent the expected behavior of $g_{FQ}(r)$ for the types of solutes and solvents studied here using a Lennard-Jones form for $w(r)$

$$w(r) = 4\varepsilon_{FQ}\left\{\left(\frac{\sigma_{FQ}}{r}\right)^{12} - \left(\frac{\sigma_{FQ}}{r}\right)^{6}\right\} \quad (20)$$

Simulations of a few nonpolar solute various ionic liquid models[83,87] suggest that $g_{FQ}(r)$ can be reasonably represented by such a function using values of σ between 0.8 and 1 times the sum of radii defined by the van der Waals volumes of the solutes and values of $\varepsilon_{FQ} \approx k_B T$. For simplicity, we use $\sigma_{FQ} = R_F + R_Q$ and allow ε_{FQ} to vary when fitting the quenching data.

The final parameter that needs to be specified is the relative diffusion coefficient D. We adopt a hydrodynamic description and relate D to the solution viscosity η via an effective hydrodynamic radius R_h in the following Stokes−Einstein relationship:

$$D = \frac{k_B T}{6\pi\eta R_h} \quad (21)$$

Quenching data are fit using measured values of η, treating R_h as an adjustable parameter. If a hydrodynamic description is correct, one expects $R_h = (R_F^{-1} + R_Q^{-1})^{-1} = 1.68$ Å.

4. RESULTS AND DISCUSSION

4.1. General Features of the Quenching Data. Steady state absorption and emission spectra of DCA in the ionic liquid $[N_{3111}][Tf_2N]$ are shown in Figure 1. Also shown for reference is the absorption spectrum of neat DMA. Two features of the fluorophore DCA make it more convenient than several other solutes we examined for these experiments. First, the S_1 absorption band of DCA lies sufficiently in the visible region of the spectrum that it is possible to excite the fluorophore (420 nm) where absorption of the DMA quencher is negligible at the concentrations employed. Second, as shown in the bottom panel of Figure 1, DCA undergoes only a very small solvation-induced dynamic Stokes shift. Lack of a significant dynamic Stokes shift means that, in contrast to the more popular coumarin dyes, the emission decays of DCA are very close to single exponential functions of time in the absence of the quencher. This feature, as well as the long lifetime of DCA (~13 ns), enables more definitive measurement of the time-dependent quenching process. As indicated by the arrows labeled obs in Figure 1, we measured emission decays at 2−4 wavelengths near the peak of the second vibronic feature in the emission of DCA and used averages over these decays for the quenching analysis.

Figure 2 shows representative steady-state spectra and time-resolved decays of DCA + DMA in $[Pr_{41}][Tf_2N]$ at 298 K. Parameters extracted from these data are summarized in Table 3. As shown here, we typically collected data at quencher concentrations near to 0, 0.05, 0.1, 0.15, and 0.2 M and use such data sets for the fits described in the following section. As illustrated in Figure 2a, the shape of the steady-state emission is invariant to quencher concentration. This invariance was observed for both emission and absorption spectra in all polar solvents studied, at least up to 0.3 M DMA. In cyclohexane, addition of DMA induced a slight redshift of the absorption spectrum, consistent with what would be expected for nonspecific solvation of DCA by DMA. As a measure of the relative intensity I of the steady-state emission, we use the integral over the range 430−500 nm and this quantity is listed in the Stern−Volmer

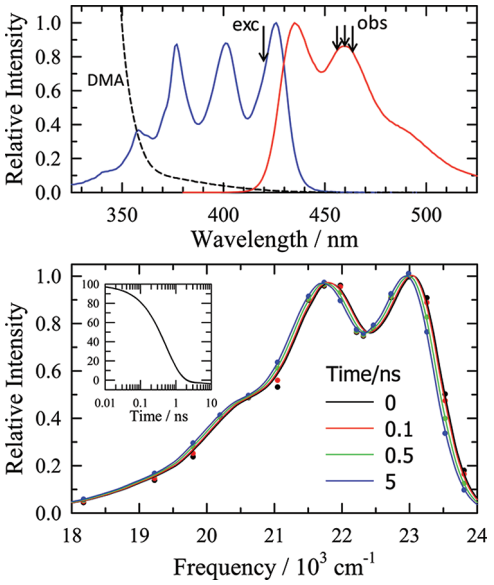

Figure 1. Steady-state (top) and time-resolved (bottom) spectra of DCA in $[N_{3111}][Tf_2N]$ at 298 K. The dashed curve in the top panel is the absorption spectrum of the DMA quencher. (Other spectra are normalized but the DMA absorption is the OD observed for neat DMA in a 1 cm cuvette.) Exc and obs indicate the excitation and observation wavelengths typically used in these experiments. The bottom panel shows time-resolved spectra obtained via spectral reconstruction (points) and fits to these data (smooth curves) assuming the time-dependent spectra to be shifted versions of the steady-state spectrum. The inset shows the frequency shift (cm^{-1}) from the steady-state spectrum versus time based on such fits.

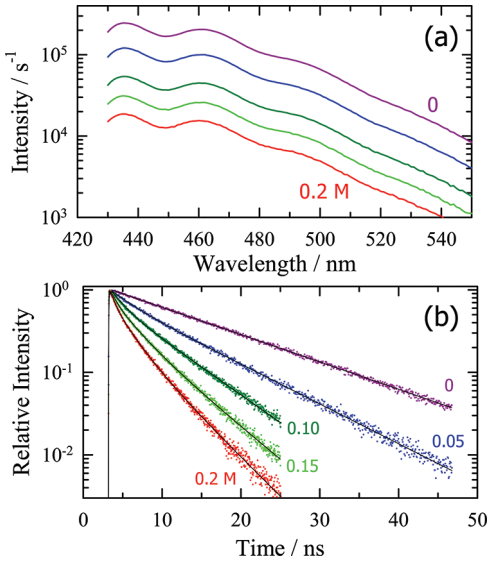

Figure 2. Representative steady-state emission spectra (a) and time-resolved decays (b; 460 nm) of DCA + DMA in $[Pr_{41}][Tf_2N]$ at 298 K. Emission spectra are shown on a logarithmic intensity scale in order to display their constant shape. These spectra are truncated on the blue edge to avoid the 420 nm excitation light. The decay data are shown normalized for easy comparison; they are collected to ~5000 counts in the peak channel. Points show the actual data and the solid black curves are multiexponential fits to these data.

dx.doi.org/10.1021/jp210892c |J. Phys. Chem. B 2012, 116, 1370–1384

Table 3. Representative Quenching Data in $[Pr_{41}][Tf_2N]$ at 298 K[a]

[DMA]	I_0/I	$I(0)$	α_1	α_2	α_3	τ_1	τ_2	τ_3	$\langle\tau\rangle$	$\tau_0/\langle\tau\rangle$
0	1.0	5077	1	0	0	13.1			13.1	1.00
0.05	2.1	4994	0.776	0.224	0	9.00	2.64		7.58	1.73
0.11	4.7	5903	0.662	0.338	0	6.46	1.67		4.84	2.71
0.16	8.2	6110	0.397	0.362	0.240	5.52	2.48	0.61	3.09	4.25
0.21	13.8	6327	0.301	0.384	0.315	4.62	2.12	0.53	2.37	5.54

[a] [DMA] is the concentration of quencher (mol dm^{-3}) and I_0/I the factor by which the steady-state emission intensity decreases compared to that in the absence of quencher. $I(0)$ and the α_i and τ_i are parameters of multi-exponential fits of the time-resolved decays to $I(t)/I(0) = \Sigma_i \alpha_i \exp(-t/\tau_i)$, $\langle\tau\rangle = \Sigma_i \alpha_i \tau_i$, and τ_0 is the lifetime in the absence of quencher. All times are in units of nanoseconds.

format I_0/I in Table 3. Decays in the presence of quencher were collected over time windows in which the intensity dropped by roughly 100-fold relative to the initial intensity in order to focus attention on the most important part of the quenching kinetics and to avoid the potential influence of impurity fluorescence from the ionic liquid solvents. Parameters of multiexponential representations of these data, derived from iterative reconvolution fitting, are also provided in Table 3. As shown there, even at 50 mM quencher concentrations, the observed decays are nonexponential. For concentrations above 0.15 M, at least three exponentials were typically required to represent such data. This nonexponentiality, which is observed in all cases studied, signals the fact that much of the observed quenching takes place in the transient portion of the overall reaction, prior to the establishment of any well-defined reaction rate constant.

Although the nonstationary character of the kinetics suggests that Stern–Volmer analysis might be misleading, to summarize the quenching data and for purposes of comparing to previous studies, we first employed a Stern–Volmer type of analysis.[32] Figure 3 shows representative Stern–Volmer plots of I_0/I and $\tau_0/\langle\tau\rangle$ versus quencher concentration in $[Pr_{41}][Tf_2N]$ at four temperatures. The $\langle\tau\rangle$ here are the integral decay times of the nonexponential decays, and τ_0 is the time constant in the absence of quencher. In keeping with the nonstationary kinetics, these plots are nearly always nonlinear.[88] As can be deduced from the different vertical scales in Figure 3, the steady state I_0/I data tend to lie above the $\tau_0/\langle\tau\rangle$ data and are usually more strongly curved. Both types of data can be accurately represented by quadratic functions of concentration

$$I_0/I = a_2[\mathrm{DMA}]^2 + a_1[\mathrm{DMA}] + 1 \quad (22a)$$

$$\tau_0/\langle\tau\rangle = b_2[\mathrm{DMA}]^2 + b_1[\mathrm{DMA}] + 1 \quad (22b)$$

Table 4 summarizes all of the data we have collected in both ionic liquid and conventional solvents in terms of such quadratic Stern–Volmer fits. Also listed in this table are values of solvent viscosity and the simple Smoluchowski predictions for the diffusion-limited rate constant k_D. If one ignores the nonlinearity of the Stern–Volmer data and simply calculates a quenching rate constant k_q from the value of $r_{SV} = I_0/I$ or $\tau_0/\langle\tau\rangle$ at some concentration via $k_q \cong (r_{SV} - 1)/[Q]\tau_0$, the rates so obtained are typically greater and often much greater than k_D. The columns labeled $(k_q/k_D)^{(x)}$ with $x = I$ or τ list the apparent enhancements over the diffusion-controlled limit based on steady-state and

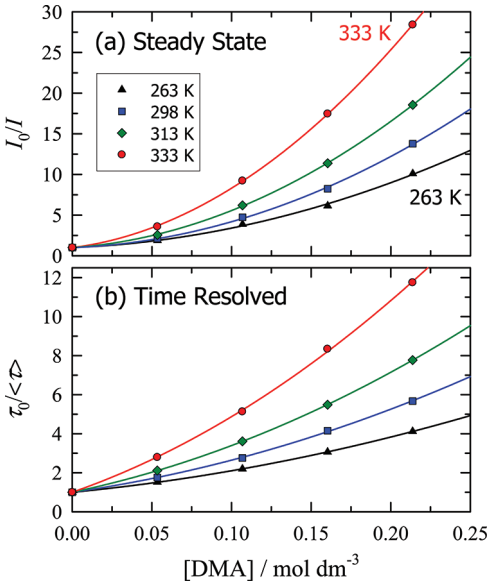

Figure 3. Stern–Volmer plots of quenching efficiencies in $[Pr_{41}][Tf_2N]$ based on (a) integral intensities from steady-state spectra and (b) integral decay times from time-resolved decays. Points are data at the indicated temperatures and solid curves are fits of these data to eqs 22a and 22b.

time-resolved data at a quencher concentration of 0.1 M. In ionic liquids, the values of (k_q/k_D) we observe are similar to the values previously found for a number of the other reactions listed in Table 1.[89] In contrast, in the low-viscosity conventional solvent acetonitrile, $(k_q/k_D) \approx 2$. As discussed in the Introduction, this difference compared to low-viscosity conventional solvents has lead previous authors to conclude that diffusion-limited electron transfer reactions are much more rapid than expected in ionic liquids, probably as a result of anomalously rapid solute diffusion. However, it can be seen from Table 4 that large values of (k_q/k_D) are not unique to ionic liquids. Conventional solvents possessing viscosities similar to those of ionic liquids show comparable values of (k_q/k_D). Moreover, as illustrated in Figure 4, there is a correlation between the value of (k_q/k_D) and solvent viscosity.

As shown in the following section, there is nothing anomalous about the rates of the DCA + DMA reaction in the ionic liquids or other high-viscosity solvents. The higher and apparently anomalous rates in ionic liquids reflect the combined effect of multiple shortcomings of the simple Smoluchowski approach for predicting effective k_q values derived from Stern–Volmer data in the case of electron transfer reactions in high-viscosity media. A more complete analysis, which considers the transient component of the reaction and uses a reasonable description of the distance dependence of electron transfer, accounts for the quenching behavior observed in all solvents.

Before discussing this analysis, it is useful to consider the meaning of the differences in the Stern–Volmer plots obtained from steady-state versus time-resolved measurements. As already noted, the extent of quenching reported by steady-state measurements is generally larger, which indicates that some portion of the quenching is missed by the time-resolved experiments due to insufficient time resolution. As shown in Figure 3, the difference between I_0/I and $\tau_0/\langle\tau\rangle$ is greater than a factor of 2 at the highest concentrations of quencher. Such large differences might be interpreted to mean that a substantial fraction of the reaction

Table 4. Stern−Volmer Characterization of Steady-State and Time-Resolved Quenching Data[a]

					SS results		TR results			comparisons at 0.1 M		
solvent[b]	T (K)	$[Q]_{max}$ (M)	η_0 (mPa s)	$k_D/10^8$ (M^{-1} s^{-1})	a_2 (M^{-2})	a_1 (M^{-1})	τ_0(ns)	b_2 (M^{-2})	b_1 (M^{-1})	$(k_q/k_D)^{(I)}$	$(k_q/k_D)^{(\tau)}$	f_{obs}
acetonitrile	298	0.30	0.34	194	2574	309	12.8	409	355	2.3	1.6	0.99
ethylene glycol	298	0.30	16	4.1	447	15.8	13.6	53	20.9	11	4.7	0.87
EGG; x_{EG} = 0.8	298	0.20	29	2.3	216	11.7	13.5	32	13.1	11	5.2	0.85
EGG; x_{EG} = 0.7	298	0.15	51	1.3	322	11.8	13.4	0	17.6	26	10	0.82
EGG; x_{EG} = 0.5	298	0.20	135	0.49	86	7.22	13.2	0	7.8	24	12	0.83
$[Pr_{31}][Tf_2N]$	298	0.17	60	1.1	348	9.18	13.1	74	16.2	31	16	0.89
$[Pr_{41}][Tf_2N]$	283	0.21	153	0.41	159	8.16	13.0	31	7.9	45	21	0.82
$[Pr_{41}][Tf_2N]$	298	0.21	74	0.89	242	7.69	13.1	48	11.6	27	14	0.86
$[Pr_{41}][Tf_2N]$	313	0.21	41	1.7	320	13.6	13.2	68	17.1	20	11	0.88
$[Pr_{41}][Tf_2N]$	333	0.21	21	3.5	486	24.6	13.4	104	28.3	15	8.2	0.91
$[Pr_{61}][Tf_2N]$	298	0.20	104	0.63	176	11.4	13.0	53	10.2	35	19	0.86
$[Pr_{81}][Tf_2N]$	298	0.30	139	0.48	173	9.19	12.9	51	16.5	43	35	0.96
$[Pr_{10,1}][Tf_2N]$	298	0.30	183	0.36	194	4.23	13.0	44	11.6	50	34	0.91
$[N_{3111}][Tf_2N]$	298	0.15	76	0.88	407	16.0	13.9	0	34.6	47	29	0.93
$[N_{10,111}][Beti]$	318	0.20	254	0.28	241	8.33	13.2	112	10.5	89	59	0.92
$[Im_{41}][PF_6]$	293	0.30	262	0.25	104	0.65	12.8	19	6.4	35	26	0.93
$[P_{14,666}][Tf_2N]$	298	0.20	346	0.19	357	43.7	12.6	56	30.7	329	151	0.90
cyclohexane	298	0.30	0.90	74	3604	113	10.6	419	210	6.1	3.2	0.98

[a] $[Q]_{max}$ is the maximum concentration of quencher examined, η_0 is the viscosity of the solvent (in the absence of quencher), and k_D is the diffusion-limited rate constant from eq 6. a_1 and a_2 and b_1 and b_2 are the parameters of eqs 22a and 22b describing the steady-state and time-resolved Stern−Volmer plots, and τ_0 is the DCA lifetime in the absence of quencher. $(k_q/k_D)^{(x)}$ are ratios of effective quenching rate constants to k_D based on steady-state ($x = I$) and time-resolved ($x = \tau$) data, and f_{obs} is the fraction of the reaction observed from the present time-resolved experiments (eq 24). [b] EGG denotes an ethylene glycol/glycerol mixture at the specified mole fraction of ethylene glycol.

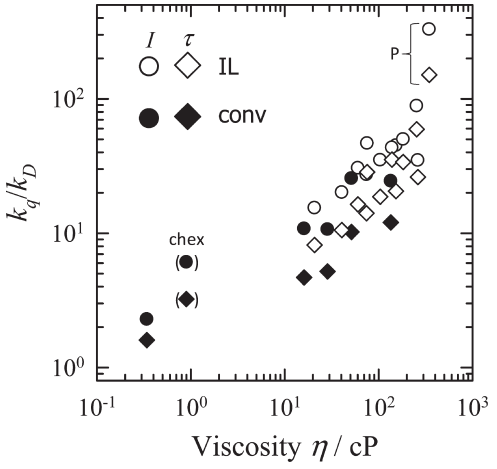

Figure 4. Correlation between the ratios of quenching rate constants k_q obtained from Stern−Volmer analyses at 0.1 M DMA to diffusion-controlled rate constant k_D. Filled and open symbols denote data in conventional solvents and ionic liquids, respectively. Circles are data from steady-state intensity measurements (I_0/I) and diamonds are data from integral decay times ($\tau_0/\langle\tau\rangle$). Chex and P denote data in cyclohexane and $[P_{14,666}][Tf_2N]$.

is too fast to be observed in the present experiments, but this is not the case. The two experiments report the fraction of excited molecules that are quenched prior to emission as

$$f_q^{(I)} = 1 - \frac{I}{I_0} \quad \text{and} \quad f_q^{(\tau)} = 1 - \frac{\langle\tau\rangle}{\tau_0} \tag{23}$$

The fraction of the molecules initially excited but not observed in the time-resolved experiments (the so-called static quenching component[32]) is the difference $f_{static} = f_q^{(I)} - f_q^{(\tau)}$. The fraction of excited molecules that *are* observed is thus

$$f_{obs} = 1 + \frac{I}{I_0} - \frac{\langle\tau\rangle}{\tau_0} \tag{24}$$

This fraction is listed in the last column of Table 4. The values of f_{obs} listed here are for 0.1 M quencher, but values are similar at other concentrations. In no case is $f_{obs} < 0.8$, and it averages 0.91 over the data set examined here. The ∼25 ps resolution of the TCSPC technique does not preclude accurately fitting the quenching data obtained here as long as this missing fraction is accounted for.

4.2. Fitting to the Reaction Model. Rather than directly fitting the observed time-resolved decays to the reaction model, we instead used multiexponential representations of the decay data such as those shown in Table 3. Data sets for each solvent and temperature were fit separately, with most sets consisting of five quencher concentrations near 0, 0.05, 0.1, 0.15, and 0.2 M. The multiexponential parametrizations of these data were used to create samples of 200 points equally spaced between 100 ps and the time at which the fluorescence dropped to 1% of its initial intensity (1−50 ns) for each quencher concentration. The starting time of 100 ps was chosen as the point where the effects of instrumental broadening were expected to be negligible after multiexponential fitting. To account for the fact that some of the early decay was missed due to limited time resolution, each sampled decay was normalized using the value of f_{obs} determined from the differences between I_0/I and $\tau_0/\langle\tau\rangle$ as described in the previous section. In addition to the decay data, estimates of the

solution viscosities as functions of composition were supplied as input. (See Supporting Information.) Fits were performed in Matlab using the nonlinear optimization routine lsqnonlin provided with this software.[90] The sum of the squared residuals (r^2) in the fitted and normalized data sets was used as the minimization criterion.

For fitting purposes, most of the twelve model parameters summarized in Table 2 were ultimately fixed at known or assumed values as described in section 3.2. Initially, the five parameters V_0, β_{el}, ΔG_0, ε_{FQ}, and R_h were considered for fitting the model to the experimental data. The electron transfer parameters V_0, β_{el}, and ΔG_0 were found to be strongly coupled and insufficiently constrained by the data to be independently varied. As already discussed, β_{el} was therefore fixed at the estimate of 1.5 Å^{-1}, despite the fact that it might be expected to depend upon solvent. V_0 represents an orientationally averaged value, which cannot be predicted with any certainty, but it is reasonably assumed to be solvent independent. Fixing ΔG_0 to -1.2 eV and allowing V_0 to vary led to best-fit values in the range $40 \leq V_0 \leq 200$ cm^{-1}. We simply chose an average value of V_0 = 100 cm^{-1} for all solvents. With these two parameters fixed, variation of ΔG_0 primarily changes the overall rate of the electron transfer reaction. The interplay between the electron transfer rate and the rate of diffusion, represented by the second variable parameter R_h, is the main determinant of the shapes of the fluorescence decays. The final variable parameter ε_{FQ}, which describes the $F-Q$ potential of mean force, determines the relative concentration of quencher near to the fluorophore at time zero. It therefore enables some adjustment of the relative rates of reaction at short and long times. To fit a given set of data, we began with V_0 = 100 cm^{-1}, β_{el} = 1.5 Å^{-1}, $\Delta G_0 = -1.2$ eV (or +0.8 eV for cyclohexane), and ε_{FQ} = 2.5 kJ/mol, and varied only R_h. Then, separate and simultaneous variations of ε_{FQ} and ΔG_0 were attempted. If the value of r^2 did not decrease by more than 25% by optimizing one of these latter parameters, the constrained value was adopted.[91]

Representative fits to the model of section 3 are shown in Figures 5 and 6, and a summary of resulting model parameters is provided in Table 5. The two data sets in Figure 5 illustrate the quality of the fits achieved for ionic liquid solvents. According to the values of the goodness-of-fit metric (r^2, Table 5) these two limiting temperatures of the $[Pr_{41}][Tf_2N]$ series represent the best (333 K) and worst (283 K) fits achieved. The first thing to be noted is that even in the best cases, the fits do not capture the sampled deconvoluted experimental data to within uncertainties. (We estimate a value $r^2 \leq 3 \times 10^{-6}$ would be obtained in such a case.) Some of this imperfect fit can be ascribed to inaccuracies in the measured quencher concentrations and in estimates of f_{obs}, both of which have an important impact on the value of r^2. This problem can be seen in the 333 K data in Figure 5 where the fit of one particular decay ([DMA] = 0.05 M; second slowest decay) appears to be incorrect by a small factor. For this decay, the measured value of f_{obs} is 0.91. Changing this value to 0.95, i.e., rescaling the experimental data at this particular quencher concentration by 4%, produces good agreement between all of the model and observed decays and reduces r^2 by a factor of 4, without causing an appreciable change in the fit parameters. Given that uncertainties in f_{obs} and $[Q]$ are expected to be on the order of a few percent, it is clear that some deviations between the model fits and the experimental data can be attributed to inaccuracies in these inputs. However, it is also clear that the model does not provide an exact representation of the experimental data in all cases. For example, in Table 5, one sees

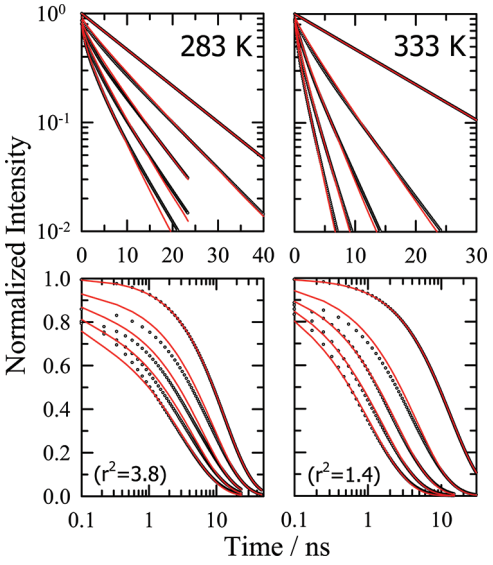

Figure 5. Fits of quenching data in $[Pr_{41}][Tf_2N]$ at 283 K (left panels) and 333 K (right panels). Sampled data are shown as points and model fits as solid curves. These two data sets represent some of the worst (283 K; $r^2 = 3.8 \times 10^{-5}$) and best (333 K; $r^2 = 1.4 \times 10^{-5}$) fits among the ionic liquids studied.

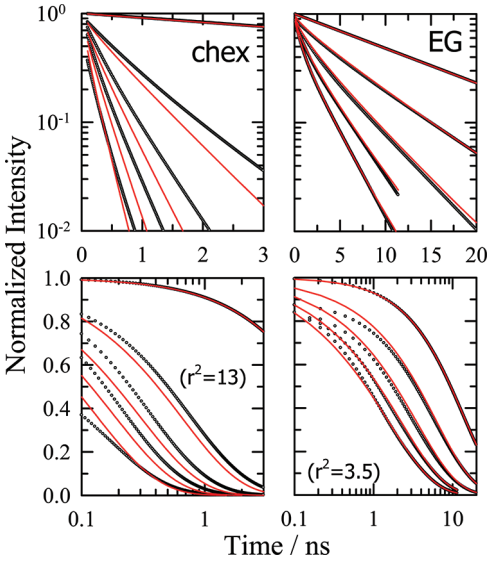

Figure 6. Fits of quenching data in cyclohexane (left panels) and ethylene glycol (right panels) at 298 K. Sampled data are shown as points and model fits as solid curves. Values of r^2 are in units of 10^{-5}.

that the value of r^2 increases systematically with decreasing temperature in the $[Pr_{41}][Tf_2N]$ series. Lowering temperature slows diffusion and the overall rate of the quenching reaction and increases the nonexponentiality of the fluorescence decays. As illustrated by the 283 K data in Figure 5, the shapes of the decays as a function of quencher concentration are imperfectly captured by the model, and deviations from experiment are larger than accounted for by combined uncertainties in $[Q]$ and f_{obs}.

Similar observations can be made for all of the other quenching data in polar solvents, for example, the ethylene glycol data shown in Figure 6. Thus, we find that the model presented in section 3 provides a good but imperfect description of the

Table 5. Summary of Fit Results[a]

	T (K)	η_0 (mPa s)	ΔG_0 (eV)	ε_{FQ} (kJ mol^{-1})	R_h (Å)	r^2 (10^{-5})	D_{DMA} (10^{-11} m^2 s^{-1})	D_{obs}/D_{SE}	R_{est}/R_h
acetonitrile	298	0.34	−1.2	4.7	0.65	0.4	323	1.6	2.6
ethylene glycol	298	16	−1.2	1.3	0.74	3.5	8.2	1.9	2.3
EGG; x_{EG} = 0.8	298	29	−1.2	2.5	0.97	3.6	3.9	1.6	1.7
EGG; x_{EG} = 0.7[b]	298	51	−1.2	3.8	0.67	1.9	2.7	2.0	2.5
EGG; x_{EG} = 0.5[b]	298	135	−1.2	5.1	0.79	2.1	1.3	2.5	2.1
[Pr_{31}][Tf_2N]	298	60	−1.2	1.4	0.46	3.7	3.7	3.2	3.7
[Pr_{41}][Tf_2N]	283	153	−1.2	2.9	0.31	3.8		3.0[c]	5.5
[Pr_{41}][Tf_2N]	298	74	−1.2	2.2	0.37	1.9	3.6	3.4	4.6
[Pr_{41}][Tf_2N]	313	41	−1.2	1.5	0.37	1.7		3.7[c]	4.5
[Pr_{41}][Tf_2N]	333	21	−1.2	1.0	0.37	1.4		4.2[c]	4.5
[Pr_{61}][Tf_2N]	298	104	−0.97	4.0	0.36	2.0	3.4	5.3	4.7
			−1.2	2.5	0.29	2.6			
[$Pr_{10,1}$][Tf_2N]	298	183	−0.97	3.9	0.24	2.9	2.4	6.3	7.0
			−1.2	2.5	0.20	3.3			
[N_{3111}][Tf_2N]	298	76	−0.87	5.8	0.23	2.7			7.2
			−1.2	3.1	0.18	3.9			
[$N_{10,111}$][Beti]	318	254	−0.87	6.5	0.17	0.2	2.9	14	9.7
			−1.2	4.0	0.11	2.6			
[Im_{41}][PF_6]	293	262	−0.89	5.0	0.37	2.5	1.4	5.2	4.5
			−1.2	3.5	0.27	4.3			
[$P_{14,666}$][Tf_2N]	298	346	−0.96	5.4	0.070	2.9	3.0	15	24
			−1.2	3.7	0.055	4.6			
cyclohexane	298	0.90	0.80	6.5	0.67	13	163	2.1	2.5
			(0.80)	(6.6)	(1.13)	(4.2)			

[a] ΔG_0, ε_{FQ}, and R_h are the model parameters described in section 3 and Table 2. r^2 is the mean squared residual of the fit, $r^2 = \sum_{i=1}^{N}(y_i^{obs} - y_i^{fit})^2/N$. D_{obs}/D_{SE} is the ratio of the measured diffusion coefficient of DMA to the Stokes−Einstein prediction $D = k_BT/6\pi R\eta$. R_{est}/R_h is the corresponding ratio of the estimated diffusion radius $R_{est} = (R_F^{-1} + R_Q^{-1})^{-1}$ = 1.68 Å and the value R_h determined from fitting the quenching data (eq 21). [b] The data for the x_{EG} = 0.7 and 0.5 mixtures only extend to 0.15 M in DMA due to limited solubility. [c] Values are estimated from temperature-dependent diffusion data on solutes other than DMA.

quenching data in high polarity solvents. The same is not true of the cyclohexane data. As shown in Figure 6, in this solvent, the concentration dependence of the decays is poorly reproduced. We note that adjusting the concentration of the 0.2 M data by ∼20% leads to an acceptable fit (data in parentheses in Table 5), perhaps suggesting that DMA association in this nonpolar solvent might be important. More study is necessary to determine the real cause of this deviation.

We now consider whether the model parameters derived from these fits (Table 5) are physically reasonable, restricting attention to the polar solvent results. As shown in Table 5, reasonable fits are achieved in most cases using the estimated value $\Delta G_0 = -1.2$ eV together with values of ε_{FQ} which average 2.9 kJ/mol. The latter values are near to k_BT, as anticipated. We note that in the series of ethylene glycol + glycerol mixtures and in the [Pr_{41}][Tf_2N] temperature series, the value of ε_{FQ} increases systematically with increasing viscosity. Rather than indicating a real change in the F−Q potential of mean force, this systematic variation probably reflects some shortcoming of the model. In addition, the quenching data in a number of the ionic liquid solvents are better fit with a smaller value of ΔG_0 near −0.9 eV and concomitantly larger values of ε_{FQ}. (ΔG_0 and ε_{FQ} are strongly correlated in these fits.) The difference between −0.9 and −1.2 eV is a larger variation in ΔG_0 than expected for these ionic liquids, and these better fits coupled to unrealistically high values of ε_{FQ} are also likely due to imperfections in the description of the quenching reaction. The final parameter R_h, which is well determined by the fits, fixes the relationship between the solution viscosity and the relative $F - Q$ diffusion coefficient. Fitted values of R_h are uniformly smaller than the value estimated from the radii of F and Q, R_{est} = 1.68 Å. There is also a clear distinction between the values of R_h in conventional and ionic liquid solvents. In conventional solvents, the ratio $R_{est}/R_h \approx 2$ (final column of Table 5), whereas in ionic liquids, this ratio is typically between 4−7 with some values, such as those in [$N_{10,111}$][Beti] and [$P_{14,666}$][Tf_2N], being much larger.

To explore whether the latter differences are actually related to differences in solute diffusion or are simply fitting artifacts, we have measured tracer diffusion coefficients of DMA in all of these solvents. The results are also provided in Table 5 along with values of D_{obs}/D_{SE}, the ratios of the measured diffusion coefficients to those estimated from the Stokes−Einstein (SE) equation, $D_{SE} = k_BT/6\pi\eta R$. As shown in Table 5, the ratios D_{obs}/D_{SE} and R_{est}/R_h parallel one another in the different solvent types. In conventional solvents $D_{obs}/D_{SE} \approx 2$, whereas larger values are found in ionic liquids. Overall, we find $R_{est}/R_h = (1.2 \pm 0.3)D_{obs}/D_{SE}$ in the conventional solvents and ionic liquids alike. Thus, the variations in R_h obtained by fitting the quenching data do appear to result from real differences in the relative $F-Q$ diffusion coefficients in different solvents, and the fact that $R_h \neq R_{est}$ is primarily a result of the inaccuracy of the SE equation. In a related study of solute diffusion,[31] we show that D_{obs}/D_{SE} increases as a function of the solvent-to-solute size ratio. (The relevance of this size ratio to diffusion has long been

recognized in the case of conventional solvents[92] and has also been noted in the case of gaseous solutes in ionic liquids.[93]) The fact that values of R_{est}/R_h and D_{obs}/D_{SE} are larger in ionic liquids than in conventional solvents can be at least partly attributed to the fact that ionic liquid ions are typically larger than molecules of many conventional organic solvents. Finally, although we did not measure diffusion coefficients of the fluorophore here, measurements of molecules of size comparable to DCA show that similar ratios of D_{obs}/D_{SE} measured for DNA should also pertain to DCA.

The foregoing discussion indicates that the model employed here provides a sound, albeit imperfect, description of the quenching of DCA by DMA. In most cases the concentration-dependent shapes of the emission profiles are semiquantitatively reproduced in both conventional and ionic liquid solvents using a consistent and physically reasonable set of electron transfer parameters. In addition, the relative diffusion coefficients derived from these fits, as embodied in the effective hydrodynamic radii R_h, are consistent with independently measured solute diffusion coefficients. Imperfections in the model are evident from the fact that deviations between observed and fitted decays are often larger than experimental uncertainties, even after accounting for the effect of uncertainties in concentrations and f_{obs}. It seems likely that better agreement with experiment could be achieved through refinement of the model. For example, more sophisticated theories of the electron transfer process,[45] an improved description of the $F-Q$ distribution function,[41] or inclusion of a distance-dependent diffusion coefficient to account for hydrodynamic interactions between F and Q[94,41] could be considered. Such improvements, whose evaluation would benefit from measurements able to capture the early dynamics (<100 ps)[95,45] not monitored here, are reserved for future studies. For now, we are satisfied that the present model is sufficiently realistic to be used to provide insight into the nature of the DCA + DMA reaction and the reasons behind the anomalous kinetics exhibited by this and similar reactions in ionic liquids.

4.3. Interpretation of the DCA + DMA Reaction. Figure 7 shows the distance dependence of the electron transfer parameters ΔG, λ, V_{el}, $\exp\{-(\Delta G + \lambda)^2/4\lambda k_B T\}$ (labeled E_a), and the total electron transfer rate constant κ. Solid curves correspond to the model as applied to polar solvents and dashed curves to the cyclohexane case. As a result of the way in which the relative permittivity enters eq 16, the reaction free energy ΔG depends little upon reactant separation in polar solvents, whereas it is strongly dependent on r in cyclohexane (Figure 7a). Just the opposite behavior occurs for the reorganization energy λ, which has zero solvent contribution in the case of cyclohexane. In both cases, $\Delta G + \lambda > 0$ at all accessible values of r, meaning that electron transfer always occurs in the normal regime. Because of the much smaller value of λ in cyclohexane, the activation energy term $\exp\{-(\Delta G + \lambda)^2/4\lambda k_B T\}$ exhibits a much steeper distance dependence than in polar solvents and is nearly equal in importance to the coupling term V_{el}^2 (Figure 7b). As a result, the net distance dependence of the electron transfer rate constant $\kappa(r)$ is considerably steeper in the case of cyclohexane. $\kappa(r)$ decreases approximately exponentially with decay constants of 1.9 and 3.0 $Å^{-1}$ in polar solvents and cyclohexane, respectively (Figure 7c). For both types of solvent, κ is predicted to achieve a rate of ~1 ps^{-1} near contact. Such a value seems plausible given the decay time of 170 fs observed for DCA in neat DMA.[95] Finally, Figure 7d illustrates $F-Q$ distributions for values of ε_{FQ} spanning the range obtained from the fits. We note that for values of ε_{FQ} as large as 5 kJ/mol (~$2k_BT$), the enhanced probability of finding an $F-Q$ pair near contact ($g^{max} \approx 8$) seems unrealistically large compared to what is observed in simulation ($g^{max} \approx 2-4$).[87,83] Such values, which are obtained in several of the fits in Table 5, probably reflect some error in the model representation at early times.

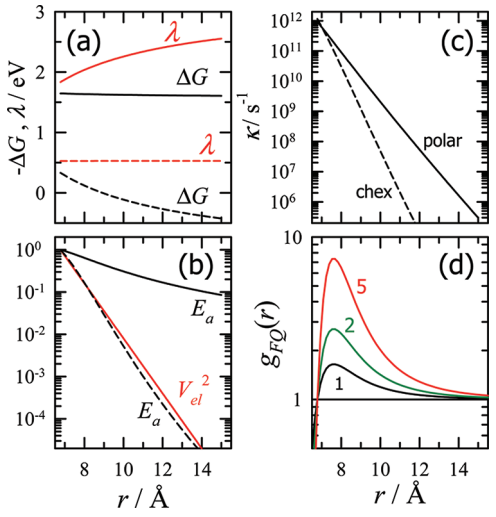

Figure 7. Some features of the electron transfer model: (a) $\Delta G(r)$ and $\lambda(r)$ (eqs 15 and 16); (b) normalized exponential terms associated with the activation energy (E_a, eq 13) and the electronic coupling (V_{el}^2, eq 14); (c) the complete electron transfer rate constant κ (eq 13). Solid curves in panels a–c show the model as applied to polar solvents and dashed curves to cyclohexane, both using the parameters specified in Table 2. (d) $F-Q$ radial distribution functions (eq 20) of the model with values of the energy parameter ε_{FQ} = 1.2, 2.5, and 5 kJ/mol at 298 K.

In Figure 8, we use standard parameters for polar solvents as listed in Table 2 to illustrate the effect that varying the viscosity has upon the time-dependent reaction rate coefficient $k(t)$ and the fluorescence decay profiles $I(t)/I(0)$. The latter are shown for a quencher concentration of 0.1 M. At times sufficiently short that no reactant motion has occurred, the rate coefficient is given by $k(0) = \langle\kappa\rangle$. As can be seen from eq 9, the initial rate constant is dictated solely by $\kappa(r)$ and the $F-Q$ distribution, $g_{FQ}(r) = \exp\{-w(r)/k_BT\}$. In the present reaction, we find $k(0) \approx 2 \times 10^{10}$ M^{-1} s^{-1}. For sufficiently rapid diffusion, represented by η = 0.1 cP in Figure 8, the equilibrium spatial distribution of $F-Q$ distances is not perturbed by the reaction. In this reaction-limited regime, $k(t)$ remains equal to $k(0)$ for all times, the overall quenching process has the well-defined bimolecular rate constant $k_q = \langle\kappa\rangle$, and $I(t)$ decays exponentially with the pseudofirst-order rate constant $k = k_0 + k_q[Q]$. For higher viscosities (slower diffusion), the initial spatial distribution can no longer be maintained during the course of the reaction. Population is depleted at small r and $k(t)$ decreases with time until the distribution becomes stationary, whereupon $k(t)$ achieves its limiting value $k(\infty)$ given by eq 8. Values of $k(\infty)$ at different viscosities are listed in the inset table in Figure 8. For sufficiently slow diffusion, the diffusion-controlled regime in which $k(\infty) = k_{DC}(\infty) \propto D \propto \eta^{-1}$ is reached. For the DCA + DMA reaction in polar solvents, this regime is achieved for η > 10 cP. Finally, it is important to recognize that, except in the reaction-controlled regime, $k(t)$ varies significantly in time, and thus, there is no unique rate constant k_q that can be associated with the reaction. For purposes of later discussion, we define an

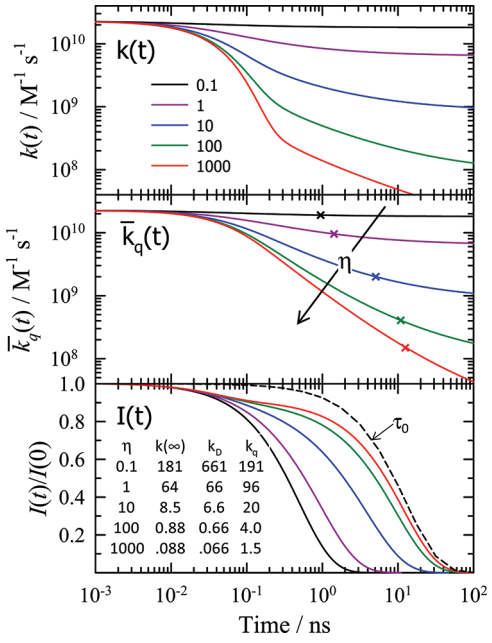

Figure 8. Model calculations illustrating the dependence of the quenching dynamics upon solution viscosity (values in mPa s). $k(t)$ is the time-dependent rate constant (eq 7), $\bar{k}_q(t)$ is the cumulative average of $k(t)$ defined in eq 25, and $I(t)/I(0)$ is the normalized fluorescence decay profile (eq 1). Parameter values are those appropriate to polar solvents listed in Table 2 with $[Q]$ = 0.1 M and τ_0 = 13 ns. The crosses in the middle panel indicate effective observation windows defined by $\bar{k}_q(t_{obs}) = (1/\langle\tau\rangle - 1/\tau_0)/[Q]$ with $\langle\tau\rangle = \int_0^\infty I(t)dt/I(0)$. The curve labeled τ_0 is the decay in the absence of quencher. The inset table compares values of the limiting rate constant at infinite time ($k(\infty)$; eq 8), the diffusion-limited rate constant k_D given by eq 6, and the effective quenching rate constant $k_q \equiv (1/\langle\tau\rangle - 1/\tau_0)/[Q]$.

average rate constant

$$\bar{k}_q \equiv \frac{1}{t_{obs}}\int_0^{t_{obs}} k(t)dt \qquad (25)$$

where t_{obs} represents the time window over which the reaction is monitored. The variation of this average rate constant with the time t_{obs} is plotted in the middle panel of Figure 8.

We now use the model calculations in Figure 8 to explain why values of the effective rate constants k_q obtained from Stern−Volmer analyses are often much larger than the simple Smoluchowski prediction $k_D = 8k_BT/3\eta$ in ionic liquids. As a representative example, we consider $[Pr_{61}][Tf_2N]$, which has a viscosity near 100 cP at 298 K. As listed in Table 4, Stern−Volmer analysis of the steady-state quenching data yields the value k_q/k_D = 35 at 0.1 M DMA for this case. There are three distinct contributions, which collectively result in k_q being much greater than k_D here. The first contribution is related to the fact that the reaction model used to derive the simple Smoluchowski prediction for k_D differs from the reaction model adopted here. The Smoluchowski approach assumes negligible $F-Q$ interactions, i.e., $w(r) = 0$ for $r > R_F + R_Q$, and it also assumes an infinitely rapid reaction but only at contact. Inclusion of a nonzero $w(r)$ and a finite, distance-dependent $\kappa(r)$ in the more complete model used here leads to the differences between $k(\infty)$ and k_D shown in the inset table in Figure 8. In the diffusion-controlled regime, which pertains to $[Pr_{61}][Tf_2N]$, these differences only increase $k(\infty)$ over k_D by a modest 34%. A second, and much more important source of error in the k_D prediction comes from the inaccuracy of the Stokes−Einstein equation for diffusion coefficients when applied to ionic liquids. The value of D_{obs}/D_{SE} = 5.3 listed in Table 5 indicates that this hydrodynamic approximation results in a value of k_D that is about 5-fold smaller than what would be obtained if, instead of SE estimates, one used measured diffusion coefficients. A final source of error lies in the fact that k_D is only an estimate for the long-time limiting rate constant pertaining after the $F-Q$ distribution has become stationary. By comparing Stern−Volmer quenching data to k_D, one implicitly assumes that little or no quenching occurs during the transient regime of the reaction. Such an assumption is typically incorrect. In the present systems, a substantial portion of the quenching occurs before a stationary distribution has been established. When $k(0)$ and $k(\infty)$ differ widely, as they do here for viscosities greater than 10 cP (Figure 8), nonexponential decays and net quenching efficiencies much greater than predicted from k_D or $k(\infty)$ are expected. For example, the effective rate constants k_q used in compiling $(k_q/k_D)^{(I)}$ values in Table 4 are defined by $k_q = (I_0/I - 1/\tau_0)/[Q]$. Such k_q values, determined from model $I(t)/I(0)$ decays for a quencher concentration of 0.1 M, are listed in the inset table to Figure 8. At a viscosity of 100 cP relevant to $[Pr_{61}][Tf_2N]$, $k_q/k(\infty)$ = 4.6. Summarizing these results, we find that the factor of 35 error in the simple Smoluchowski prediction for the extent of reaction results from the multiplicative effect of three factors: (i) a factor of ~1.3 due to neglect of the nonuniform initial $F-Q$ distribution and the distance dependence of electron transfer, (ii) a factor of ~5 due to inaccuracy of the SE prediction of diffusion coefficients, and (iii) another factor of ~5 due to the fact that much of the reaction occurs during the nonstationary regime.

We finally ask how viscosity and other experimental variables influence the last of these three sources of deviation in k_q/k_D. To do so, it is helpful to define an effective time window t_{obs} over which quenching experiments monitor reaction. We define this time by $\bar{k}_q(t_{obs}) \equiv (1/\langle\tau\rangle - 1/\tau_0)/[Q]$. Such times for $[Q]$ = 0.1 M are marked as crosses in the middle panel of Figure 8. From this figure, one finds that with decreasing viscosity, the reaction becomes faster, and t_{obs} becomes shorter. With this truncation of the observation window, k_q approaches $k(0)$, and one might therefore expect k_q to be even farther from the diffusion-controlled limit $k(\infty)$, but because the difference between $k(0)$ and $k(\infty)$ lessens with decreasing viscosity, the net effect is to cause $k_q/k(\infty)$ to decrease relative to its value at high viscosities. For this reason, although equating k_q to $k(\infty)$ as is done in the simple Smoluckowski approach often appears to be a good approximation in low viscosity solvents, it becomes progressively worse as viscosity increases. This effect is the primary reason for the variation of k_q/k_D with η shown in Figure 4. Quencher concentration and fluorophore lifetime τ_0 also affect the observation window and thus affect how much k_q departs from $k(\infty)$. For η = 100 cP and $[Q]$ = 0.1 M, one finds that $t_{obs} \approx \tau_0$, i.e., it is the fluorophore lifetime that mainly limits the extent of reaction. For τ_0 = 1, 10, 100 ns, values of $k_q/k(\infty)$ = 19, 5, and 2. Thus, other things being equal, a longer-lived fluorophore achieves effective quenching rates closer to the diffusion limit. If the quencher concentration is increased beyond 0.1 M at η = 100 cP, it is the reaction rate that limits the observation window. For example, changing $[Q]$ from 0.1 to 1 M causes the observation window to decrease from ~11 ns to ~1 ns and $k_q/k(\infty)$ to increase from 4.6 to 16.

These observations provide some insight into the wide range of values of k_q/k_D listed in Table 1. First, we note that for

reactions measured in multiple ionic liquids having widely differing viscosities (#5, 6, 7, and 8) values of k_q/k_D increase with increasing viscosity similarly to what is shown in Figure 4. (See Table S3, Supporting Information.) Presumably, the interpretation of this behavior is the same as that just described for the DCA + DMA reaction. For a number of reactions examined in high viscosity ionic liquids (#6−8), values of k_q/k_D are modest, less than 10 in most cases. Common to these cases is the fact that observations were made at low reactant concentrations and with reactants whose lifetimes are relatively long. Under such conditions, the observation window is not limited to short times and the measurements do not tend to emphasize the transient portion of the reaction. In contrast, extreme values of k_q/k_D (#1, 3, and 5) in Table 1 are limited to high-viscosity systems in which solute lifetimes and/or high concentrations emphasize the portions of $k(t)$ occurring well before stationary conditions apply. These observations are also consistent with the foregoing analysis.[96] For example, using the model parameters in Table 2 with η = 100 cP, τ_0 = 1 ns, and [Q] = 1 M and assuming $D_{obs}/D_{SE} \approx 5$, one finds $k_q/k_D \approx 200$, a value comparable to the most extreme values in Table 1. Thus, it seems reasonable to expect that detailed analyses of the sort described here, taking into account the specifics of the electron transfer processes involved as well as the underestimation of diffusion coefficients by Stokes−Einstein predictions, would provide satisfactory explanations for what appear to be widely variable and sometimes unexpectedly high reaction rates reported for diffusion-limited reactions in ionic liquids.

5. SUMMARY AND CONCLUSIONS

We have studied the electron transfer reaction between S_1 DCA and DMA using steady-state and picosecond time-resolved emission techniques in both ionic liquids and conventional solvents. Our primary interest was to better understand why diffusion-limited electron transfer reactions sometimes appear to be much faster than expected based on viscosity scaling the rates observed in conventional solvents.

For the quencher concentrations examined here (<0.3 M), emission decays are significantly nonexponential and Stern−Volmer plots of steady-state intensities and (integral) lifetimes far from linear in ionic liquid solvents. These features indicate that reaction does not involve a simple kinetic process. Application of the usual Stern−Volmer (SV) analysis to such data yields results qualitatively similar to what was previously reported by Vieira and Falvey[26] for this particular reaction and by others for similar singlet quenching processes. Even at concentrations of 0.1 M in DMA, effective quenching rate constants k_q determined in this manner are much larger than the simple Smoluchowski predictions for diffusion-limited reactions, $k_D = 8k_BT/3\eta$. Values of k_q/k_D greater than 10 are typical, and values greater than 100 are observed in some cases. But such large departures from the k_D prediction are not a unique feature of ionic liquids. We also observed $k_q \gg k_D$ in conventional solvents having viscosities comparable to those of ionic liquids. Moreover, a general correlation between k_q/k_D and viscosity was noted. Understanding the origin of these departures from k_D predictions and, indeed, even the meaning of these k_q values requires further analysis.

We therefore also considered a more complete description of the quenching process, using a model that combines solution of a spherical diffusion equation coupled to a Marcus-type description of the electron transfer reaction. Such modeling has been applied to reactions in conventional solvents[36−45] but had not been previously considered for reactions in ionic liquids. Using this approach, we were able to obtain satisfactory fits of the concentration-dependent fluorescence decay profiles observed in both ionic liquid and conventional solvents using a consistent set of physically reasonable parameters. The model developed for the DCA + DMA reaction showed that there are two main reasons why the k_q values obtained from SV analysis are often much greater than k_D in ionic liquids. First, conditions of high viscosity (slow diffusion) emphasize the transient portions of reaction, i.e., those portions occurring prior to establishment of steady-state conditions where the rate coefficient $k(t)$ is still time-dependent. k_D is only a prediction for the limiting time constant $k(t \rightarrow \infty)$, and the latter constant is smaller than $k(t)$ at any earlier time. Stern−Volmer analysis provides an effective rate constant k_q, which can be viewed as an average of $k(t)$ over some time window set by a combination of the net quenching rate and the fluorophore lifetime. k_q is therefore necessarily larger than $k(\infty)$, whose estimate is k_D. In high viscosity (η > 100 cP) solvents and for the conditions employed here, we estimate that $k_q/k(\infty)$ lies in the range of 5−10. Even larger values are expected for experiments conducted with higher quencher concentrations and/or shorter fluorophore lifetimes.

The second important contributor to large values of k_q/k_D is the fact that the Stokes−Einstein relationship, $D_{SE} = k_BT/6\pi\eta R$, assumed in deriving the simple Smoluchowski prediction for k_D, significantly underestimates diffusion coefficients in ionic liquids. This effect was suggested by the small effective hydrodynamic radii required to fit the quenching data to the model and confirmed by direct measurements of the diffusion of DMA in all of the solvents studied. The ratio D_{obs}/D_{SE} is largely determined by the relative sizes of solute and solvent molecules,[31] and the large size of ionic liquid constituents makes these ratios larger than in most conventional solvents. Values of D_{obs}/D_{SE} in the range 3−5 are typical in ionic liquids, but values larger than 10 are observed for ionic liquids comprising the largest cations studied. These diffusion factors multiply the factors of $k_q/k(\infty)$ caused by transient effects, so that together, quite large values of k_q/k_D can be obtained.

We have only considered one particular reaction in this study and have applied what can be viewed as a minimally realistic model for treating bimolecular electron transfer reactions. Nevertheless, it seems likely that foregoing interpretations suffice to account for other cases in which surprisingly large values of k_q (i.e., $k_q \gg k_D$) have been reported. No special character of electron transfer need be postulated to explain such observations. Furthermore, while solute diffusion *is* faster than Stokes−Einstein estimates in ionic liquids, values of D_{obs}/D_{SE} cannot be inferred directly from k_q/k_D and are unlikely to be as large as originally thought based on quenching experiments.

■ ASSOCIATED CONTENT

Supporting Information. Description of temperature dependent viscosities and the effect of DMA on viscosities and diffusion coefficients and an expanded version of Table 1. This material is available free of charge via the Internet at http://pubs.acs.org.

■ AUTHOR INFORMATION

Corresponding Author
*E-mail: maroncelli@psu.edu.

■ ACKNOWLEDGMENT

We are indebted to Attila Szabo for helpful discussions concerning application of the formalism of ref 46. This work was funded by the Division of Chemical Sciences, Geosciences, and Biosciences, Office of Basic Energy Sciences of the U.S. Department of Energy through grant DE-FG02-09ER16118.

■ REFERENCES

(1) Wishart, J. F. *Energy Environ. Sci.* **2009**, *2*, 956.
(2) Armand, M.; Endres, F.; MacFarlane, D. R.; Ohno, H.; Scrosati, B. *Nat. Mater.* **2009**, *8*, 621.
(3) Lin, R.; Taberna, P.-L.; Fantini, S.; Presser, V.; Perez, C. R.; Malbosc, F.; Rupesinghe, N. L.; Teo, K. B. K.; Gogotsi, Y.; Simon, P. *J. Phys. Chem. Lett.* **2011**, *2*, 2396.
(4) Shim, Y.; Jung, Y.; Kim, H. J. *J. Phys. Chem. C* **2011**, *115*, 23574.
(5) Lewandowski, A.; Swiderska-Mocek, A. *J. Power Sources* **2009**, *194*, 601.
(6) Zakeeruddin, S. M.; Graetzel, M. *Adv. Funct. Mater.* **2009**, *19*, 2187.
(7) Kawano, R.; Katakabe, T.; Shimosawa, H.; Nazeeruddin, M. K.; Graetzel, M.; Matsui, H.; Kitamura, T.; Tanabe, N.; Watanabe, M. *Phys. Chem. Chem. Phys.* **2010**, *12*, 1916.
(8) Hapiot, P.; Lagrost, C. *Chem. Rev.* **2008**, *108*, 2238.
(9) Barrosse-Antle, L. E.; Bond, A. M.; Compton, R. G.; O'Mahony, A. M.; Rogers, E. I.; Silvester, D. S. *Chem. Asian J.* **2010**, *5*, 202.
(10) Khoshtariya, D. E.; Dolidze, T. D.; van Eldik, R. *Chem.—Eur. J.* **2009**, *15*, 5254.
(11) Endres, F.; Hoefft, O.; Borisenko, N.; Gasparotto, L. H.; Prowald, A.; Al-Salman, R.; Carstens, T.; Atkin, R.; Bund, A.; Zein, E. A. S. *Phys. Chem. Chem. Phys.* **2010**, *12*, 1724.
(12) Lynden-Bell, R. M. *J. Phys. Chem. B* **2007**, *111*, 10800.
(13) Shim, Y.; Kim, H. J. *J. Phys. Chem. B* **2007**, *111*, 4510.
(14) Shim, Y.; Kim, H. J. *J. Phys. Chem. B* **2009**, *113*, 12964.
(15) Annapureddy, H. V. R.; Margulis, C. J. *J. Phys. Chem. B* **2009**, *113*, 12005.
(16) Li, X.; Liang, M.; Chakraborty, A.; Kondo, M.; Maroncelli, M. *J. Phys. Chem. B* **2011**, *115*, 6592.
(17) Castner, E. W., Jr.; Margulis, C. J.; Maroncelli, M.; Wishart James, F. *Annu. Rev. Phys. Chem.* **2011**, *62*, 85.
(18) Samanta, A. *J. Phys. Chem. Lett.* **2010**, *1*, 1557.
(19) Maroncelli, M.; Zhang, X.-X.; Liang, M.; Roy, D.; Ernsting, N. P. *Faraday Discuss. Chem. Soc.* **2012**, *154*, 409.
(20) Gordon, C. M.; McLean, A. J. *Chem. Commun.* **2000**, 1395.
(21) McLean, A. J.; Muldoon, M. J.; Gordon, C. M.; Dunkin, I. R. *Chem. Commun.* **2002**, 1880.
(22) Skrzypczak, A.; Neta, P. *J. Phys. Chem. A* **2003**, *107*, 7800.
(23) Grampp, G.; Kattnig, D.; Mladenova, B. *Spectrochim. Acta, Part A* **2006**, *63A*, 821.
(24) Takahashi, K.; Sakai, S.; Tezuka, H.; Hiejima, Y.; Katsumura, Y.; Watanabe, M. *J. Phys. Chem. B* **2007**, *111*, 4807.
(25) Paul, A.; Samanta, A. *J. Phys. Chem. B* **2007**, *111*, 1957.
(26) Vieira, R. C.; Falvey, D. E. *J. Phys. Chem. B* **2007**, *111*, 5023.
(27) Sarkar, S.; Pramanik, R.; Seth, D.; Setua, P.; Sarkar, N. *Chem. Phys. Lett.* **2009**, *477*, 102.
(28) Sarkar, S.; Pramanik, R.; Ghatak, C.; Rao, V. G.; Sarkar, N. *Chem. Phys. Lett.* **2011**, *506*, 211.
(29) Takahashi, K.; Tezuka, H.; Kitamura, S.; Satoh, T.; Katoh, R. *Phys. Chem. Chem. Phys.* **2010**, *12*, 1963.
(30) Das, A. K.; Mondal, T.; Sen, M. S.; Bhattacharyya, K. *J. Phys. Chem. B* **2011**, *115*, 4680.
(31) Kaintz, A.; Benesi, A.; Baker, G.; Maroncelli, M. 2012, manuscript in preparation.
(32) Lakowicz, J. R. *Principles of Fluorescence Spectroscopy*, 3rd ed.; Springer: New York, 2006.
(33) Nitzan, A. *Chemical Dynamics in Condensed Phases; Relaxation, Transfer, and Reactions in Condensed Molecular Systems*; Oxford: New York, 2006.
(34) Szabo, A. *J. Phys. Chem.* **1989**, *93*, 6929.
(35) Burshtein, A. I. *Adv. Chem. Phys.* **2004**, *129*, 105.
(36) Murata, S.; Matsuzaki, S. Y.; Tachiya, M. *J. Phys. Chem.* **1995**, *99*, 5354.
(37) Murata, S.; Tachiya, M. *J. Phys. Chem.* **1996**, *100*, 4064.
(38) Iwai, S.; Murata, S.; Tachiya, M. *J. Chem. Phys.* **1998**, *109*, 5963.
(39) Burel, L.; Mostafavi, M.; Murata, S.; Tachiya, M. *J. Phys. Chem. A* **1999**, *103*, 5882.
(40) Swallen, S. F.; Weidemaier, K.; Tavernier, H. L.; Fayer, M. D. *J. Phys. Chem.* **1996**, *100*, 8106.
(41) Swallen, S. F.; Weidemaier, K.; Fayer, M. D. *J. Chem. Phys.* **1996**, *104*, 2976.
(42) Weidemaier, K.; Tavernier, H. L.; Swallen, S. F.; Fayer, M. D. *J. Phys. Chem. A* **1997**, *101*, 1887.
(43) Rosspeintner, A.; Kattnig, D. R.; Angulo, G.; Landgraf, S.; Grampp, G.; Cuetos, A. *Chem.—Eur. J.* **2007**, *13*, 6474.
(44) Rosspeintner, A.; Kattnig, D. R.; Angulo, G.; Landgraf, S.; Grampp, G. *Chem.—Eur. J.* **2008**, *14*, 6213.
(45) Angulo, G.; Kattnig, D. R.; Rosspeintner, A.; Grampp, G.; Vauthey, E. *Chem.—Eur. J.* **2010**, *16*, 2291.
(46) Dudko, O. K.; Szabo, A. *J. Phys. Chem. B* **2005**, *109*, 5891.
(47) Jin, H.; O'Hare, B.; Dong, J.; Arzhantsev, S.; Baker, G. A.; Wishart, J. F.; Benesi, A.; Maroncelli, M. *J. Phys. Chem. B* **2008**, *112*, 81.
(48) Kilaru, P.; Baker, G. A.; Scovazzo, P. *J. Chem. Eng. Data* **2007**, *52*, 2306.
(49) Gardecki, J. A.; Maroncelli, M. *Appl. Spectrosc.* **1998**, *52*, 1179.
(50) Heitz, M. P.; Maroncelli, M. *J. Phys. Chem. A* **1997**, *101*, 5852.
(51) Wu, D.; Chen, A.; Johnson, C. S., Jr. *J. Magn. Reson.* **1995**, *115*, 260.
(52) The dimensions of the various rate parameters discussed here are not immediately obvious from the equations. By letting $[x]$ denote the dimensions of the quantity x and using the notation l = length, t = time, and n = amount of substance, the dimensions can be expressed: $[k_0] = [k(r)] = t^{-1}$, $[k(t)] = [k_D] = [k(\infty)] = [\langle\kappa\rangle] = [k_{DC}] = n^{-1}l^{+3}t^{-1}$. Thus, the former quantities are unimolecular rate parameters, and the latter quantities are bimolecular rate parameters.
(53) Krissinel, E. B.; Agmon, N. *J. Comput. Chem.* **1996**, *17*, 1085.
(54) Smoluchowski, M. *Z. Phys. Chem.* **1917**, *92*, 129.
(55) Laidler, K. *Chemical Kinetics*; Harper Collins: New York, 1987.
(56) Steinfeld, J. I.; Francisco, J. S.; Hase, W. L. *Chemical Kinetics and Dynamics*; Plenum Press: Englewood Cliffs, NJ, 1989.
(57) A factor of 2 is missing in the expression for $\alpha_{1,2}$ given as eq 21c of ref 46. Equation 11 is the corrected version. Attila Szabo, private communication.
(58) Marcus, R. A.; Sutin, N. *Biochim. Biophys. Acta* **1985**, *811*, 265.
(59) Barzykin, A. V.; Frantsuzov, P. A.; Seki, K.; Tachiya, M. *Adv. Chem. Phys.* **2002**, *123*, 511.
(60) Marcus, R. A. *J. Chem. Phys.* **1956**, *24*, 966.
(61) Miyazaki, K.; Tachiya, M. *J. Chem. Phys.* **1998**, *109*, 7424.
(62) Rehm, D.; Weller, A. *Isr. J. Chem.* **1970**, *8*, 259.
(63) Edwards, J. T. *J. Chem. Educ.* **1970**, *47*, 261.
(64) The reorganization energy was calculated from the sum of the vertical energies $\{E(F^-)_{F^*} - E(F^-)_{F-}\} + \{E(Q^+)_Q - E(Q^+)_{Q+}\}$ where $E(A1)_{A2}$ denotes the energy of A1 in the equilibrium geometry of A2.
(65) Castner, E. W., Jr.; Kennedy, D.; Cave, R. J. *J. Phys. Chem. A* **2000**, *104*, 2869.
(66) Scherer, P. O. J. *J. Phys. Chem. A* **2000**, *104*, 6301.
(67) Scherer, P. O. J.; Tachiya, M. *J. Chem. Phys.* **2003**, *118*, 4149.
(68) Wenger, O. S. *Acc. Chem. Res.* **2011**, *44*, 25.
(69) Wenger, O. S.; Leigh, B. S.; Villahermosa, R. M.; Gray, H. B.; Winkler, J. R. *Science* **2005**, *307*, 99.
(70) Miller, J. R.; Beitz, J. V.; Huddleston, R. K. *J. Am. Chem. Soc.* **1984**, *106*, 5057.
(71) Eriksen, J.; Foote, C. S. *J. Phys. Chem.* **1978**, *82*, 2659.
(72) Gould, I. R.; Ege, D.; Moser, J. E.; Farid, S. *J. Am. Chem. Soc.* **1990**, *112*, 4290.
(73) Kikuchi, K.; Hoshi, M.; Niwa, T.; Takahashi, Y.; Miyashi, T. *J. Phys. Chem.* **1991**, *95*, 38.

(74) Jones, G.; Griffin, S. F.; Choi, C. Y.; Bergmark, W. R. *J. Org. Chem.* **1984**, *49*, 2705.
(75) Burget, D.; Jacques, P.; Vauthey, E.; Suppan, P.; Haselbach, E. *J. Chem. Soc. Faraday Trans.* **1994**, *90*, 2481.
(76) Shirota, H.; Pal, H.; Tominaga, K.; Yoshihara, K. *J. Phys. Chem. A* **1998**, *102*, 3089.
(77) Huang, M.-M.; Jiang, Y.; Sasisanker, P.; Driver, G. W.; Weingärtner, H. *J. Chem. Eng. Data* **2011**, *56*, 1494.
(78) Kobrak, M. N.; Li, H. *Phys. Chem. Chem. Phys.* **2010**, *12*, 1922.
(79) Poole, C. F. *J. Chromatogr., A* **2004**, *1037*, 49.
(80) Reichardt, C. *Green Chem.* **2005**, *7*, 339.
(81) Acree, W. E., Jr.; Abraham, M. H. *J. Chem. Technol. Biotechnol.* **2006**, *81*, 1441.
(82) Jin, H.; Baker, G. A.; Arzhantsev, S.; Dong, J.; Maroncelli, M. *J. Phys. Chem. B* **2007**, *117*, 7291.
(83) Roy, D.; Maroncelli, M. 2011, manuscript in preparation.
(84) Lynden-Bell, R. M. *J. Chem. Phys.* **2008**, *129*, 204503/1.
(85) Lee, H. Y.; Issa, J. B.; Isied, S. S.; Castner, E. W., Jr.; Pan, Y.; Hussey, C. L.; Lee, K. S.; Wishart, J. F. *J. Phys. Chem.* **2011**in press.
(86) Castner, E. W., Jr.; Santos, C. S. 2011, private communication.
(87) Examples of simulated $w(r)$ for spherical solutes in an all-atom model of $[Im_{21}][Tf_2N]$ are provided inPaschek, D.; Koeddermann, T.; Ludwig, R. *Phys. Rev. Lett.* **2008**, *100*, 115901.
(88) This observation of nonlinear Stern−Volmer plots is at odds with the results of Vieira and Falvey.[26] These authors reported steady-state Stern−Volmer plots for the quenching of DCA by a variety of amines including DMA to be linear over concentration ranges of 0.4−1.2 M in $[Im_{41}][PF_6]$ and $[Im_{81}][PF_6]$. We extended the measurements of DCA + DMA in $[Im_{41}][PF_6]$ reported in Table 4 to the range 0.05−1.2 M in order to make more direct comparison to the Vieira and Falvey work but found highly nonexponential Stern−Volmer plots. The reason for this discrepancy is not known.
(89) Our value of $(k_q/k_D) = 35$ for the DCA + DMA reaction in $[Im_{41}][PF_6]$ at 0.1 M DMA differs significantly from $(k_q/k_D) = 85$ calculated from the value of k_q reported by Vieira and Falvey[26] for this identical system. However, the latter authors measured quenching at higher DMA concentrations where the nonlinearity of the Stern−Volmer plots makes the effective rate constant k_q much larger.
(90) For evaluating the complementary error function in eq 7, whose argument is often complex, we used a routine for numerical evaluation of the Faddeeva function $\exp(-z^2)erfc(-iz)$ described inWeideman, J. A. C. Computation of the Complex Error Function. *SIAM J. Numer. Anal.* **1994**, *31*, 1497–1518.The Matlab routine for this function was written by Kesh Ikuma and is available at http://www.mathworks.com/matlabcentral/fileexchange/22207-faddeeva-function-fft-based.
(91) We note that Tachiya and co-workers[36] previously measured the quenching of DCA by DMA in ethylene glycol and fit time-resolved emission decays to a model nearly identical to the one employed here. The main difference compared to the present model is that they assumed $w(r) = 0$. They adopted the fixed parameters $R_F = 3.7$, $R_Q = 3.2$ Å, $R_H = 1.72$ Å, and $\Delta G_0 = -1.21$ eV. For DMA concentrations of 0.25 (0.31) M, they achieved best fit to their data using the electron transfer parameters $V_0 = 22$ (37) cm^{-1} and $\beta_{el} = 0.9$ (1.0) $Å^{-1}$.
(92) Gierer, A.; Wirtz, K. *Z. Naturforsch.* **1953**, *8a*, 532.
(93) Ferguson, L.; Scovazzo, P. *Ind. Eng. Chem. Res.* **2007**, *46*, 1369.
(94) Northrup, S. H.; Hynes, J. T. *J. Chem. Phys.* **1979**, *71*, 871.
(95) Iwai, S.; Murata, S.; Katoh, R.; Tachiya, M.; Kikuchi, K.; Takahashi, Y. *J. Chem. Phys.* **2000**, *112*, 7111.
(96) One aspect of the data in Table 1 that seems contrary to expectations is the difference between k_q/k_D in systems 2 and 3. These data are for quenching of coumarins C151 and C152 by DMA in two different ionic liquids. They were recorded by a single research group using the same methods.[27,28] It is difficult to rationalize why large values of k_q/k_D should be observed in the moderate viscosity liquid (DAF) at relatively low quencher concentrations when much more modest values are observed in $[Im_{21}][Tf_2N]$.